PROCEEDINGS OF SCIENCE

Angular analysis of $\mathrm{B} \to \mathrm{K}^{(*)}\mu\mu$ decays at CMS

Alessio Boletti*, **on behalf of the CMS Collaboration**
Universita' degli studi di Padova & INFN
E-mail: alessio.boletti@cern.ch

The flavour changing neutral current decays are interesting probes for new physics searches. The angular distributions of $b \to s\ell^+\ell^-$ transition processes of both $\mathrm{B}^0 \to \mathrm{K}^{*0}\mu^+\mu^-$ and $\mathrm{B}^+ \to \mathrm{K}^+\mu^+\mu^-$ decays are studied using a sample of proton-proton collisions at $\sqrt{s} = 8$ TeV collected with the CMS detector at the LHC, corresponding to an integrated luminosity of 20.5 fb^{-1}. Angular analyses are performed to determine the angular parameters P_1 and P_5' for $\mathrm{B}^0 \to \mathrm{K}^{*0}\mu^+\mu^-$ and A_{FB} and F_H parameters for $\mathrm{B}^+ \to \mathrm{K}^+\mu^+\mu^-$, as functions of the dimuon invariant mass squared. All the measurements are consistent with the standard model predictions. In addition, the projections for the sensitivity of the measurement of the P_5' parameter in the $\mathrm{B}^0 \to \mathrm{K}^{*0}\mu^+\mu^-$ angular analysis at the High-Luminosity LHC is reported.

18th International Conference on B-Physics at Frontier Machines - Beauty2019 -
29 September / 4 October, 2019
Ljubljana, Slovenia

*Speaker.

PoS(Beauty2019)030

1. Introduction

Phenomena beyond the Standard Model (SM) can be probed directly, via the production of new particles, or indirectly, by studying the production and decay of SM particles. The transitions of the type $b \to s\ell^+\ell^-$ are flavor-changing neutral currents (FCNCs). According to the SM, these transitions are forbidden at tree level and occur through higher-order processes penguin or box diagrams. For this reason, the measurement of these rare FCNC decays is very sensitive to physics phenomena beyond the SM.

The Compact Muon Solenoid Experiment (CMS) has analysed two FCNC decays: $B^0 \to K^{*0}\mu^+\mu^-$, where K^{*0} indicates the $K^{*0}(892)$ meson, and $B^+ \to K^+\mu^+\mu^-$ [1, 2]. Both analyses use a data sample collected in proton-proton (pp) collisions at a centre-of-mass energy of 8 TeV with the CMS detector at LHC, corresponding to an integrated luminosity of 20.5 fb^{-1}.

2. The $B^0 \to K^{*0}\mu^+\mu^-$ decay

The angular distribution of the $B^0 \to K^{*0}\mu^+\mu^-$ decay can be described as a function of four kinematic variables: the dimuon invariant mass squared, q^2, the decay angle of the dimuon system, θ_ℓ, the decay angle of the K^{*0}, θ_K, and the angle between these two decay planes, φ.

Among several angular parameters used to describe the angular decay rate of the $B^0 \to K^{*0}\mu^+\mu^-$ process, the P_5' parameter is of particular interest due to LHCb and Belle measurements [3, 4, 5] that indicate a potential discrepancy with the standard model. CMS performed a measurement of the P_1 and P_5' angular parameters [1], trying to elucidate the situation.

In the measurement, the q^2 spectrum, ranging from 1 to 19 GeV^2, has been divided in 9 bins, and the values of P_1 and P_5' angular parameters are determined by fitting the distribution of events as a function of the three angular variables, independently in each q^2 bin. The q^2 bins $8.68 < q^2 < 10.09\ GeV^2$ and $12.90 < q^2 < 14.18\ GeV^2$, contain the $B^0 \to K^{*0}J/\psi$ and $B^0 \to K^{*0}\psi(2S)$ decays, respectively, and are used as control channels to validate the analysis.

The angular distribution of $B^0 \to K^{*0}\mu^+\mu^-$ can be written as:

$$\begin{aligned}\frac{1}{d\Gamma/dq^2}\frac{d^4\Gamma}{dq^2 d\cos\theta_\ell d\cos\theta_K d\varphi} = \frac{9}{8\pi}\Bigg\{&\frac{2}{3}\Big[(F_S + A_S\cos\theta_K)\left(1-\cos^2\theta_\ell\right) + A_S^5\sqrt{1-\cos^2\theta_K}\sqrt{1-\cos^2\theta_\ell}\cos\varphi\Big]\\ &+(1-F_S)\Big[2F_L\cos^2\theta_K\left(1-\cos^2\theta_\ell\right) + \frac{1}{2}(1-F_L)\left(1-\cos^2\theta_K\right)\left(1+\cos^2\theta_\ell\right)\\ &+\frac{1}{2}P_1(1-F_L)(1-\cos^2\theta_K)(1-\cos^2\theta_\ell)\cos 2\varphi\\ &+2P_5'\cos\theta_K\sqrt{F_L(1-F_L)}\sqrt{1-\cos^2\theta_K}\sqrt{1-\cos^2\theta_\ell}\cos\varphi\Big]\Bigg\}\end{aligned} \tag{2.1}$$

where F_L denotes the longitudinal polarisation fraction of the K^{*0}, F_S represents the contamination fraction of spin 0 (S-wave) $B^0 \to K^-\pi^+\mu^+\mu^-$ decays, and A_S and A_S^5 encode the interference between S-wave and P-wave. This expression is an exact simplification of the full angular distribution, obtained by folding the φ and θ_ℓ variables around zero and $\pi/2$, respectively.

For each q^2 bin, the observables of interest are extracted from an unbinned extended maximum-likelihood fit to four variables: the $K^-\pi^+\mu^+\mu^-$ invariant mass, m, and the three angular variables,

$\cos\theta_\ell$, $\cos\theta_K$, and φ. The probability density function (pdf) used in the fit has the following expression:

$$\begin{aligned}\text{p.d.f.}(m,\cos\theta_\mathrm{K},\cos\theta_\ell,\varphi) = Y_S^C \cdot \Big(& S^R(m)\cdot S^a(\cos\theta_\mathrm{K},\cos\theta_\ell,\varphi)\cdot \varepsilon^R(\cos\theta_\mathrm{K},\cos\theta_\ell,\varphi) \\ & + \frac{f^M}{1-f^M}\cdot S^M(m)\cdot S^a(-\cos\theta_\mathrm{K},-\cos\theta_\ell,-\varphi)\cdot \varepsilon^M(\cos\theta_\ell,\cos\theta_\mathrm{K},\varphi)\Big) \\ & + Y_B \cdot B^m(m)\cdot B^{\cos\theta_\mathrm{K}}(\cos\theta_\mathrm{K})\cdot B^{\cos\theta_\ell}(\cos\theta_\ell)\cdot B^\varphi(\varphi). \end{aligned} \tag{2.2}$$

where the three lines correspond to correctly tagged signal events, mistagged signal events, and background events, respectively. The parameters Y_S^C and Y_B are the yields of correctly tagged signal events and background events, respectively, and are free parameters in the fit. The parameter f^M is the fraction of signal events in which the mass assignment to the kaon and pion candidates is wrong, and is determined from MC simulation. The signal mass shapes, $S^R(m)$ and $S^M(m)$, are each the sum of two Gaussian functions sharing the same mean, and describe the mass distribution for correctly tagged and mistagged signal events, respectively.

In the signal mass shapes, the mean, the four Gaussian σ parameters, and two fractions relating the contribution of each Gaussian, are determined from simulation. The function $S^a(\cos\theta_\mathrm{K},\cos\theta_\ell,\varphi)$ describes the angular decay rate of the signal and corresponds to Equation 2.1. The functions $B^m(m)\cdot B^{\cos\theta_\mathrm{K}}(\cos\theta_\mathrm{K})\cdot B^{\cos\theta_\ell}(\cos\theta_\ell)\cdot B^\varphi(\varphi)$ are obtained from B^0 sideband data and describe the background distributions, where the mass shape is an exponential function and the angular shapes are polynomials ranging from first to fourth degree, depending on the q^2 bin and on the angular variable. The three-dimensional functions $\varepsilon^R(\cos\theta_\mathrm{K},\cos\theta_\ell,\varphi)$ and $\varepsilon^M(\cos\theta_\ell,\cos\theta_\mathrm{K},\varphi)$ parametrise the efficiencies of signal events for correctly tagged and mistagged signal events, respectively. They have been built using a novel non-parametric algorithm based on kernel density estimators.

The fit is performed in two steps: the first step uses the data from the sidebands of the B^0 mass to obtain the parameters of the background components. These parameters are then kept fixed in the second step, in which the full mass range is fitted, using the whole pdf. The free parameters in this second step are the angular parameters P_1, P_5', and A_S^5, and the yields Y_S^C and Y_B. The angular parameters F_L, F_S, and A_S are fixed to previous CMS measurements performed on the same data set with the same event selection criteria [6].

The fit algorithm is validated through fits to pseudo-experimental samples, MC simulation samples, and control channels. To ensure correct coverage for the uncertainties of the angular parameters, the Feldman-Cousins (FC) method is used to determine the statistical uncertainties of the measurements. Several sources of systematic uncertainties are evaluated, and included in the resulting uncertainty.

As an example, the projections of the fit result for the second q^2 bin, are shown in Figure 1.

The fit results of P_1 and P_5', for each q^2 bin, are shown in Figure 2, along with the SM predictions and the experimental results of other experiments. The results are consistent with the predictions based on the Standard Model.

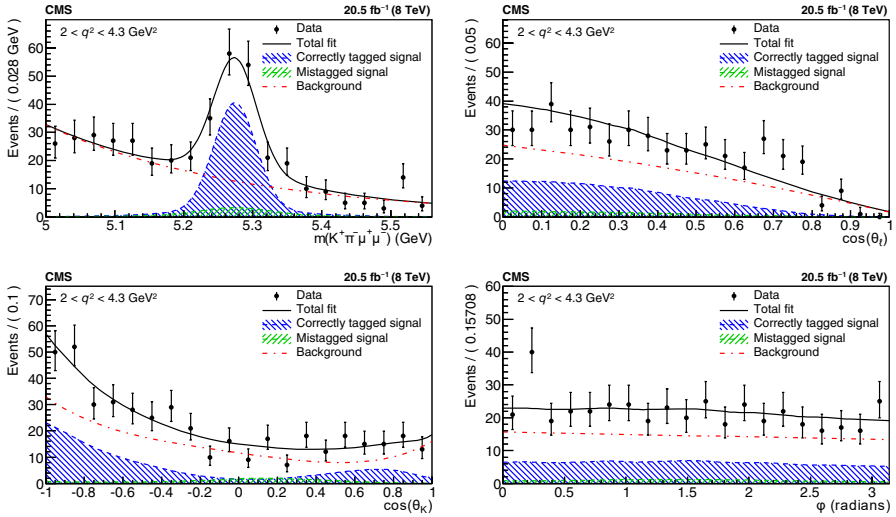

Figure 1: Invariant mass and angular distributions of $K^-\pi^+\mu^+\mu^-$ events for $2 < q^2 < 4.3$ GeV^2. The projection of the results from the total fit, as well as for correctly tagged signal events, mistagged signal events, and background events, are also shown. The vertical bars indicate the statistical uncertainties. Figure from [1].

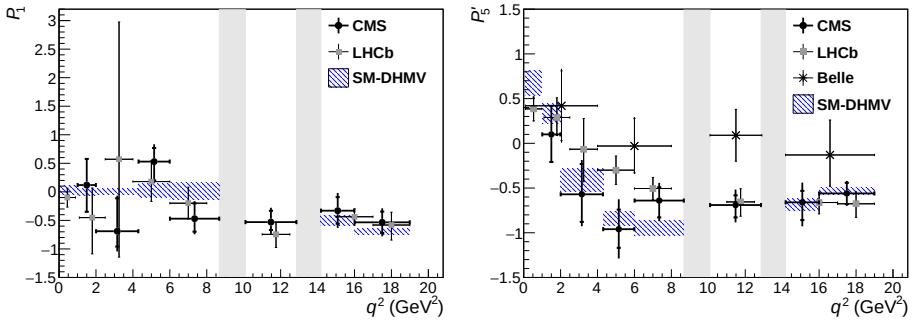

Figure 2: CMS measurements of the P_1 and P_5' angular parameters versus q^2 for $B^0 \to K^{*0}\mu^+\mu^-$ decays, in comparison to results from the LHCb [4] and Belle [5] Collaborations. The statistical uncertainties are shown by the inner vertical bars, while the outer vertical bars give the total uncertainties. The horizontal bars show the bin widths. The vertical shaded regions correspond to the J/ψ and $\psi(2S)$ resonances. The hatched region shows the predictions from two SM calculations described in the text, averaged over each q^2 bin. Figure from [1].

3. The $B^+ \to K^+\mu^+\mu^-$ decay

The angular distribution of the process $B^+ \to K^+\mu^+\mu^-$ can be described as a function of the dimuon invariant mass, q^2, and the decay angle of the dimuon system, θ_ℓ. The θ_ℓ dependence of the decay rate can be parametrised in terms of A_{FB} and F_H angular parameters, as:

$$\frac{1}{d\Gamma/dq^2}\frac{d^2\Gamma}{dq^2 d\cos\theta_\ell} = \frac{3}{4}(1-F_H)\left(1-\cos^2\theta_\ell\right) + \frac{1}{2}F_H + A_{FB}\cos\theta_\ell \tag{3.1}$$

The requirement for the decay rate to be positive in the whole phase space constrains the parameter values to satisfy $0 \leq F_H \leq 3$ and $|A_{FB}| \leq \min(1, F_H/2)$.

In this analysis, each event is reconstructed through the decay into the fully charged final state of one charged hadron and a pair of oppositely charged muons. Dimuon candidates are formed from two oppositely charged muons, that match the muon candidates that triggered the event readout. To discriminate signal events from background contamination, selection criteria on kinematic variables are used. These criteria are determined through a maximisation of the expected signal significance in the final B^+ meson invariant mass fitting region, $5.1 - 5.6$ GeV.

The q^2 spectrum, ranging from 1 to 22 GeV^2, has been divided in 9 bins; two of them containing the resonant $B^+ \to K^+ J/\psi$ and $B^+ \to K^+ \psi(2S)$ decays are used as control channels. In addition the analysis is repeated in two special bins: the first one ranges from 1 to 6 GeV^2 and includes the region with more robust theoretical predictions, and the second one includes the whole q^2 spectrum excluding the two bins of the control regions. The angular parameters A_{FB} and F_H are extracted from a two-dimensional unbinned extended maximum-likelihood fit to the B^+ candidate mass, m, and to the $\cos\theta_\ell$ distributions, in each q^2 range. The probability density function (pdf) used in the fit is:

$$\text{p.d.f.}(m, \cos\theta_\ell) = Y_S \cdot S(m) \cdot S^a(\cos\theta_\ell) \cdot \varepsilon(\cos\theta_\ell) + Y_B \cdot B^m(m) \cdot B^{\cos\theta_\ell}(\cos\theta_\ell) \tag{3.2}$$

where the two contributions correspond to the parametrisation of the signal and background. The Y_S and Y_B parameters are the yields of signal and background events, respectively. The functions $S(m)$ and $S^a(\cos\theta_\ell)$ describe the signal invariant mass and angular distributions, while $B^m(m)$ and $B^{\cos\theta_\ell}(\cos\theta_\ell)$ functions describe the background distributions. The function $\varepsilon(\cos\theta_\ell)$ encodes the signal efficiency as a function of $\cos\theta_\ell$, and is parametrised as a sixth-order polynomial whose parameters are determined through a fit to MC simulations.

The signal mass shape $S(m)$ is modelled as the sum of two Gaussian functions with a common mean, and the angular shape $S^a(\cos\theta_\ell)$ is given in Equation 3.1. The background mass shape $B^m(m)$ is modelled as a single exponential function, while the background angular shape $B^{\cos\theta_\ell}(\cos\theta_\ell)$ is parametrised as the sum of a Gaussian function and a third- or fourth-degree polynomial, depending on the q^2 bin. The free parameters of the fit are the yields, Y_S and Y_B, the angular parameters, A_{FB} and F_H, and the exponential decay parameter of $B^m(m)$.

To validate the efficiency description derived from simulation, the ratio of the branching fractions of the two control channels is compared with the world-average value. The fitting procedure has been validated using MC simulated samples. Several sources of systematic uncertainties are considered in this analysis, and included in the resulted uncertainty.

The projections of the fit results for the $K^+\mu^+\mu^-$ invariant mass and $\cos\theta_\ell$ distributions, for the special q^2 bin of $1 - 6$ GeV^2, are shown in Figure 3. To evaluate the statistical uncertainties of A_{FB} and F_H, the profiled FC technique has been used. The systematic and statistical uncertainties are added in quadrature to obtain the total uncertainty.

The measured values of A_{FB} and F_H are shown in Figure 4. The results for A_{FB} are consistent with the SM expectation of no asymmetry. The F_H values are compared with the SM predictions and a good agreement is observed. The results of this analysis are also in agreement with the previous measurements from other experiments.

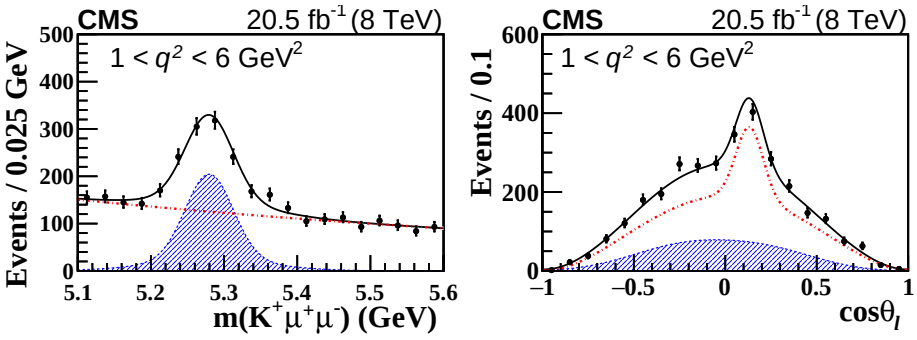

Figure 3: Projection of the $K^+\mu^+\mu^-$ invariant mass (left) and $\cos\theta_\ell$ (right) distributions for $1 < q^2 < 6$ GeV^2 from the two-dimensional fit of data. The solid lines show the total fit, the shaded area the signal contribution, and the dash-dotted lines the background. The vertical bars on the points represent the statistical uncertainty in data. Figure from [2].

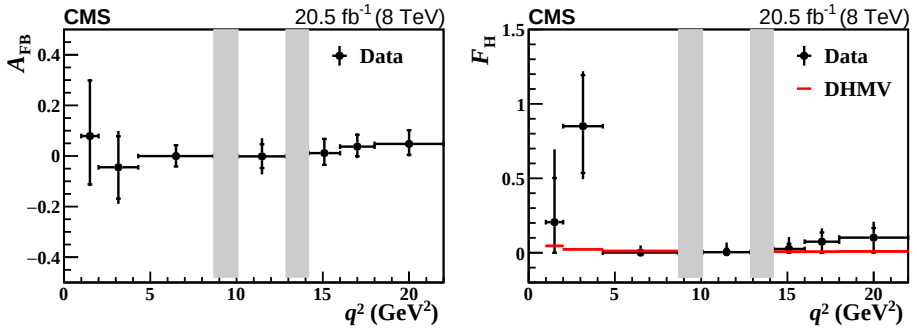

Figure 4: Results of the A_{FB} (left) and F_H (right) measurements in ranges of q^2. The statistical uncertainties are shown by the inner vertical bars, while the outer vertical bars give the total uncertainties. The horizontal bars show the q^2 range widths. The vertical shaded regions are 8.68-10.09 and 12.86-14.18 GeV^2, corresponding to the J/ψ- and $\psi(2S)$-dominated control regions, respectively. The horizontal lines in the right plot show the DHMV SM theoretical predictions [7, 8], whose uncertainties are smaller than the line width. Figure from [2].

4. Prospects for P_5' measurement at the High-Luminosity LHC

The High-Luminosity LHC (HL-LHC) run is expected to deliver about $3\,\text{ab}^{-1}$ of integrated luminosity, in pp collisions at centre of mass energy of 14 TeV [9]. Relevant improvements of the CMS detector are planned for HL-LHC [10], in order to efficiently acquire data in its challenging operating conditions. In particular, a silicon detector with extended rapidity coverage, improved granularity, and higher radiation tolerance will be installed. This is expected to provide a significant improvement in the mass-measurement resolutions, and a better signal-over-background ratio in the reconstructed decay channels.

Using the result of the CMS analysis on 2012 data as baseline, a study has been performed to estimate the expected precision of the P_5' measurement at the integrated luminosity of $3\,\text{ab}^{-1}$ [11]. For simplicity, in this study the signal-to-background ratio and the trigger thresholds and efficiencies are assumed to be unchanged with respect to the 2012 analysis, and effects of possible improvements in the analysis strategy have not be considered.

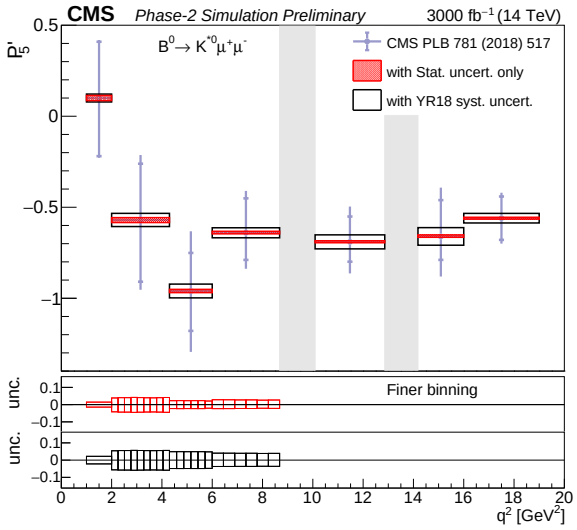

Figure 5: Projected statistical (hatched regions) and total (open boxes) uncertainties on the P_5' parameter versus q^2 in the Phase-2 scenario with an integrated luminosity of 3000 fb^{-1}. The CMS measurement of P_5' on 2012 data is shown by circles with inner vertical bars representing the statistical uncertainties and outer vertical bars representing the total uncertainties. The vertical shaded regions correspond to the J/ψ and ψ' resonances. The two lower pads represent the statistical (upper pad) and total (lower pad) uncertainties with the finer q^2 binning. Figure from [11].

Samples of simulated signal events with Phase-2 conditions are used. In each q^2 bin, the signal yield is extracted performing a maximum likelihood fit to the B^0-candidate mass spectrum, and extrapolating to an integrated luminosity of 3 ab^{-1}. The statistical uncertainty and the systematic uncertainties that are directly dependent on data statistics are obtained by scaling the correspondent uncertainties from the 2012 analysis by the square root of the 2012 over HL-LHC signal-yield ratio. The other systematic uncertainties are scaled by a factor of 2. Overall, the uncertainties are reduced down to a factor of 15 compared to the 2012 results, as shown in Figure 5. Since these projected results are dominated by the systematic uncertainties, finer q^2 bins could be used with no relevant degradation of the precision of the measurements. An additional study has been performed, by splitting some of the q^2 bins in finer bins such that the statistical an systematical uncertainties are approximately equal, as shown in the bottom pads of Figure 5.

5. Conclusions

The results of the angular analyses performed for the decays of $B^0 \to K^{*0}\mu^+\mu^-$ and $B^+ \to K^+\mu^+\mu^-$, using pp collision data recorded at $\sqrt{s} = 8$ TeV with the CMS detector corresponding to an integrated luminosity of 20.5 fb^{-1}, are presented here. In each region of the dimuon invariant mass squared, unbinned maximum-likelihood fits were applied to the distributions of the B meson invariant mass and the angular variables, to extract the values of the angular parameters. The results are consistent with previous measurements and with the predictions from the Standard Model. Finally, the projections for the sensitivity of the measurement of the P_5' parameter in the $B^0 \to K^{*0}\mu^+\mu^-$ angular analysis at the High-Luminosity LHC has been presented.

References

[1] A. M. Sirunyan *et al.* [CMS Collaboration], Phys. Lett. B **781** (2018) 517 doi:10.1016/j.physletb.2018.04.030 [arXiv:1710.02846 [hep-ex]].

[2] A. M. Sirunyan *et al.* [CMS Collaboration], Phys. Rev. D **98** (2018) 112011 doi:10.1103/PhysRevD.98.112011 [arXiv:1806.00636 [hep-ex]].

[3] R. Aaij *et al.* [LHCb Collaboration], Phys. Rev. Lett. **111** (2013) 191801 doi:10.1103/PhysRevLett.111.191801 [arXiv:1308.1707 [hep-ex]].

[4] R. Aaij *et al.* [LHCb Collaboration], JHEP **1602** (2016) 104 doi:10.1007/JHEP02(2016)104 [arXiv:1512.04442 [hep-ex]].

[5] S. Wehle *et al.* [Belle Collaboration], Phys. Rev. Lett. **118** (2017) no.11, 111801 doi:10.1103/PhysRevLett.118.111801 [arXiv:1612.05014 [hep-ex]].

[6] V. Khachatryan *et al.* [CMS Collaboration], Phys. Lett. B **753** (2016) 424 doi:10.1016/j.physletb.2015.12.020 [arXiv:1507.08126 [hep-ex]].

[7] S. Descotes-Genon, L. Hofer, J. Matias and J. Virto, JHEP **1412** (2014) 125 doi:10.1007/JHEP12(2014)125 [arXiv:1407.8526 [hep-ph]].

[8] S. Descotes-Genon, L. Hofer, J. Matias and J. Virto, JHEP **1606** (2016) 092 doi:10.1007/JHEP06(2016)092 [arXiv:1510.04239 [hep-ph]].

[9] G. Apollinari, I. BÃl'jar Alonso, O. BrÃijning, P. Fessia, M. Lamont, L. Rossi and L. Tavian, CERN Yellow Report CERN 2017-007-M doi:10.23731/CYRM-2017-004.

[10] D. Contardo, M. Klute, J. Mans, L. Silvestris and J. Butler, report: CERN-LHCC-2015-010 `https://cds.cern.ch/record/2020886`.

[11] CMS Collaboration, report: CMS-PAS-FTR-18-033 (2018) `https://cds.cern.ch/record/2651298`.